PRIMUS: GALAXY ENVIRONMENT ON THE QUIESCENT FRACTION EVOLUTION AT $Z < 0.8$

ChangHoon Hahn[1], Michael Blanton[1], Alison Coil[2], Richard Cool[3], Daniel Eisenstein[4], John Moustakas[5], Ken Wong[6], Guangtun Zhu[7]

Draft version October 9, 2014

ABSTRACT

We investigate the effects of galaxy environment on the evolution of the quiescent fraction (f_Q) from $z = 0.8$ to 0.0 using spectroscopic redshifts and multi-wavelength imaging data from the PRism MUlti-object Survey (PRIMUS) and the Sloan Digitial Sky Survey (SDSS). Our stellar mass limited galaxy sample consists of $\sim 13,000$ PRIMUS galaxies within $z = 0.2 - 0.8$ and $\sim 64,000$ SDSS galaxies within $z = 0.05 - 0.12$. We classify the galaxies as quiescent or star-forming based on an evolving specific star formation cut, and as low or high density environments based on fixed cylindrical aperture environment measurements on a volume-limited Environment Definition Population (from PRIMUS and SDSS). For quiescent and star-forming galaxies in low or high density environments, we examine the evolution of their stellar mass function (SMF) evolution. Then using the SMFs we compute the $f_Q(\mathcal{M}_*)$ and quantify the evolution of $f_Q(\mathcal{M}_*)$ within our redshift range. We find that in both low and high density environments the quiescent fraction increases with cosmic time. Moreover, we illustrate that galaxy populations in high density environments have significantly higher quiescent fractions than galaxy populations in low density environments. Furthermore, by comparing the quiescent fraction evolutions in the environments, we find that the quiescent fraction evolves noticeably more for galaxy populations in high density environments. These results suggest that environment dependent quenching has a moderate effect on the quiescent fraction evolution. Furthermore our results provide constraints on the effect of environment on star-formation quenching.

1. INTRODUCTION

Galaxies, in their detailed properties, carry the imprints of their surroundings, with a strong dependence of the quiescent fraction of galaxies on their local environment (e.g. Hubble 1936; Oemler 1974; Dressler 1980; Hermit et al. 1996; Guzzo et al. 1997; for a recent review see Blanton & Moustakas 2009). The strength of this dependence is itself a strongly decreasing function of galaxy stellar mass; at the extreme, the lowest mass ($< 10^9 \ M_\odot$) galaxies are quenched only in dense regions, and never in isolation (Geha et al. 2012). These effects vary with redshift at least in the densest clusters, as observed in the changing fraction of late-type spirals relative to the field found in studies of the morphology-density relation (Dressler 1984; Desai et al. 2007). Clearly understanding the properties of galaxies in the present-day universe requires a careful investigation of the role of environment, and how that role changes over time.

Nevertheless, the evolution of the role of environment is a relatively subtle effect and difficult to study. Al-

though history of galaxies prior to $z \sim 1$ appears to have been one of rapid assembly, since that time the galaxy population has continued to evolve, but less dramatically. Although there are detectable changes in the population, the major classes of galaxies existed at $z \sim 1$, in roughly the same relative numbers as today (Bundy et al. 2006; Borch et al. 2006; Taylor et al. 2009; Moustakas et al. 2013). Furthermore, at those redshifts we can also detect the dependence of galaxy properties on environment, with lower star-formation rate early-type galaxies populating the denser regions (Cooper et al. 2008; Patel et al. 2009; Kovač et al. 2010).

The most dramatic change in galaxy properties during the past eight billion years has been a remarkable decline in the star-formation rate of galaxies in the Universe (Hopkins & Beacom 2006). This decline appears dominated by decreases in the rates of star-formation of individual galaxies (Noeske et al. (2007)). There is evidence that a large fraction of the decline is associated with strongly infrared-emitting starbursts (Bell et al. 2005; Magnelli et al. 2009). The decline does not appear to be due to the quenching of a large fraction of the star-forming population, as reflected in observations of the stellar mass function of quiescent and star-forming galaxies (Blanton et al. 2006; Bundy et al. 2006; Borch et al. 2006; Moustakas et al. 2013). These findings leave little room for the participation of environmentally-driven quenching in the global census of star-formation. As Cooper et al. (2008) and others have pointed out, because the environmental dependence of total star-formation rates at fixed redshift is relatively small, environmentally effects are unlikely to cause the overall star-formation rate decline.

Thus, the impact of environment on galaxy forma-

[1] Center for Cosmology and Particle Physics, Department of Physics, New York University, 4 Washington Place, New York, NY 10003
[2] Center for Astrophysics and Space Sciences, Department of Physics, University of California, 9500 Gilman Dr., La Jolla, CA 92093
[3] MMT Observatory, University of Arizona, 1540 E Second Street, Tucson AZ 85721
[4] Harvard-Smithsonian Center for Astrophysics, 60 Garden Street, Cambridge, MA 02138
[5] Department of Physics and Astronomy, Siena College, 515 Loudon Road, Loudonville, NY 12211
[6] Steward Observatory, University of Arizona, 933 North Cherry Avenue, Tucson, AZ 85721
[7] Department of Physics and Astronomy, The Johns Hopkins University, 3400 North Charles Street, Baltimore, MD 21218

tion has to be interpreted on top of the background of this overall decline affecting galaxies in all environments. The most straightforward investigation would be to directly determine the star-forming properties of galaxies as a function of environment, stellar mass and redshift in a single, consistently analyzed data set. This analysis can reveal how galaxies are quenched in the universe over time, quantitatively establish the contribution of environmental effects to the overall trends, and reveal whether those trends happen equally in all environments. However, such an analysis has not been done previously due to the lack of sufficiently large samples. In this paper, we apply this approach using the Prism Multi-object Survey (PRIMUS; Coil et al. (2011), Cool et al. (2013)), the largest available redshift survey covering the epochs between $0 < z < 1$.

In Section 2 we present a brief description of the PRIMUS and SDSS data, our mass complete sample construction, and galaxy environment measurements. After dividing our galaxy sample into subsamples of star-forming or quiescent and high or low density environments, we compute and examine the evolution of the stellar mass functions for our subsamples in Section 3. Afterwards, in Section 4, we calculate the quiescent fraction, analyze the evolution of the quiescent fraction, quantify the effects of environment on the quiescent fraction evolution, and discuss the implications of our quiescent fraction results on star-formation quenching. Finally in Section 5 we summarize our results.

Throughout the paper we assume cosmology with $\Omega_m = 0.3, \Omega_\Lambda = 0.7$, and $H_0 = 70$ km s^{-1}Mpc^{-1}.

2. SAMPLE SELECTION

We are interested in quantifying the effects of galaxy environment on the evolution of the quenched fraction over the redshift range $0 < z < 1$. For our analysis, we require a sample with sufficient depth and robustness to probe the redshift range and to measure galaxy environment. PRIMUS with its $\sim 120,000$ spectroscopic redshifts provides a large data set at intermediate redshifts for our analysis. In addition, we anchor our analysis at intermediate redshifts with a low redshift sample derived from the Sloan Digital Sky Survey (York et al. (2000)).

In Section 2.1 and Section 2.2 we provide a brief summary of the PRIMUS data and the SDSS data used for our sample selection. Then in Section 2.4 we define our stellar mass complete galaxy sample. Afterwards, in Section 2.3, we classify our sample galaxies as quiescent or star-forming then calculate the environment using a volume-limited Environment Defining Population in Section 2.5. Finally in Section 2.6, we correct our galaxy sample and environment measurements for edge effects of the surveys.

2.1. PRIMUS

At intermediate redshifts we use multiwavelength imaging and spectroscopic redshifts from PRIMUS, a faint galaxy survey with $\sim 120,000$ redshifts ($\sigma_z/(1 + z) \approx 0.5\%$) within the range $z \approx 0 - 1.2$. The survey was conducted using the IMACS spectrograph on the Magellan I Baade 6.5 m telescope with a slitmask and low dispersion prism. For details on the PRIMUS observation methods such as survey design, targeting, and data

summary, we refer readers to the survey papers (Coil et al. 2011; Cool et al. 2013).

While the PRIMUS survey targeted seven distinct extragalactic deep fields for a total of ~ 9 deg^2, we restrict our sample to five fields that have $GALEX$ and $Spitzer$/IRAC imaging for a total of ~ 5.5 deg^2 (similar to the sample selection in Moustakas et al. 2013). Four of these fields are a part of the $Spitzer$ Wide-area Infrared Extragalactic Survey (SWIRE[8]): the European Large Area ISO Survey - South 1 field (ELAIS-S1[9]), the Chandra Deep Field South SWIRE field (CDFS), and the XMM Large Scale Structure Survey field (XMM-LSS). The XMM-LSS consists of two separate but spatially adjacent fields: the Subaru/XMM-Newton DEEP Survey field (XMM-SXDSS[10]) and the Canadian-France-Hawaii Telescope Legacy Survey field (XMM-CFHTLS[11]). Our fifth and final field is the Cosmic Evolution Survey (COSMOS[12]) field. For all of our fields we have near-UV (NUV) and far-UV (FUV) photometry from the $GALEX$ Deep Imaging Survey (DIS; Martin et al. 2005; Morrissey et al. 2005) as well as ground-based optical and $Spitzer$/IRAC mid-infrared photometric catalogs. Moustakas et al. (2013) provides detailed descriptions of integrated flux calculations in the photometric bands for each of our fields.

Finally, using the spectroscopic redshift and broad wavelength photometry we apply iSEDfit, a Bayesian SED modeling code, to calculate stellar masses and star formation rates (SFRs) for our sample galaxies (Moustakas et al. 2013). iSEDfit uses the redshift and the observed photometry of the galaxies to determine the statistical likelihood of a large ensemble of generated model SEDs. The model SEDs are generated using Flexible Stellar Population Synthesis (FSPS) models (Conroy & Gunn 2010) based on the Chabrier (2003) IMF, along with other prior parameters discussed in Section 4.1 and Appendix A of Moustakas et al. (2013). For the observed photometry, we use the $GALEX$ FUV and NUV, the two shortest IRAC bands at 3.6 and 4.5μm (the two longer-wavelength IRAC channels are excluded because iSEDfit does not model hot dust or polycyclic aromatic hydrocarbons emission lines), and the optical bands.

2.2. SDSS-GALEX

At low redshifts, we use spectroscopic redshifts and $ugriz$ photometry from the SDSS Data Release 7 (DR7; Abazajian et al. 2009). More specifically we select galaxies from the New York University Value-Added Galaxy Catalog (hereafter VAGC) that satisfy the main sample criterion and have galaxy extinction corrected Petrosian magnitudes $14.5 < r < 17.6$ and spectroscopic redshifts within $0.01 < z < 0.2$ (Blanton et al. 2005). We further restrict the VAGC sample to only galaxies with medium depth observations with total exposure time greater than 1 ks from $GALEX$ Release 6. This leaves $167,727$ galaxies.

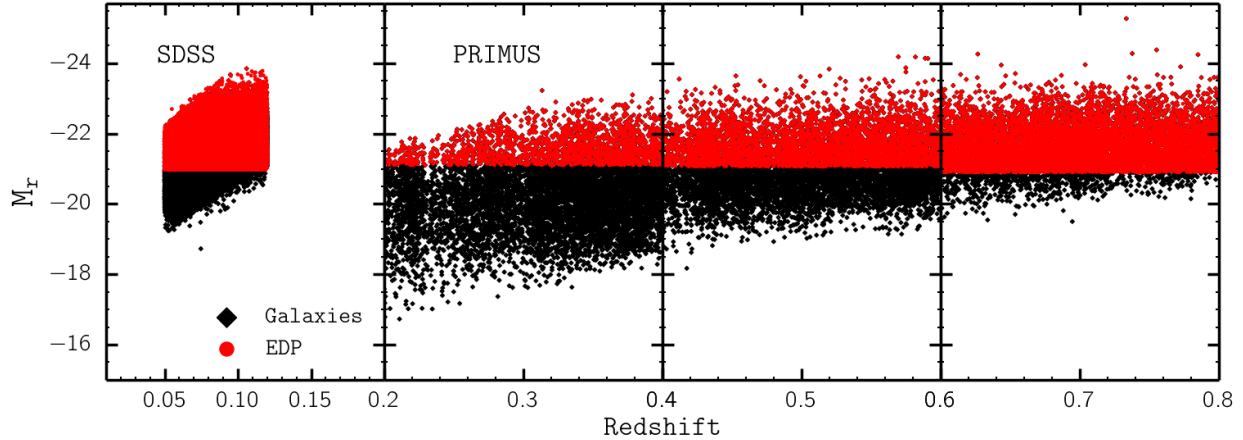Next, we use the MAST/CasJobs[13] interface and a $4''$

FIG. 1.— Absolute magnitude M_r versus redshift for our mass complete galaxy sample (black squares) with the Environment Defining Population (red circles) plotted on top. Both samples are divided into redshift bins: $z \approx 0.05 - 0.12$, $0.2 - 0.4$, $0.4 - 0.6$, and $0.6 - 0.8$ (panels left to right). The lowest redshift bin ($z \approx 0.05-0.12$; leftmost panel) contain our galaxy sample and EDP selected from SDSS. The rest contain galaxies and EDP selected from PRIMUS. The redshift limits for the lowest redshift bin are empirically selected based on the bright and faint limits of SDSS galaxies. Stellar mass completeness limits, specified in Section 2.4, are imposed on the galaxy population. Meanwhile, M_r limits are applied to the EDP such that the number density in each panel are equivalent (Section 2.5).

diameter search radius, to obtain the NUV and FUV photometry for the SDSS-$GALEX$ galaxies. For optical photometry, we use the $ugriz$ bands from the SDSS model magnitudes scaled to the r-band cmodel magnitude. These photometric bands are then supplemented with integrated JHK_s magnitudes from the 2MASS Extended Source Catalog (XSC; Jarrett et al. 2000) and with photometry at 3.4 and 4.6μm from the WISE All-Sky Data Release[14]. Further details regarding the SDSS-$GALEX$ sample photometry can be found in Section 2.4 of Moustakas et al. (2013). As previously done on the PRIMUS data in Section 2.1, we use iSEDfit to obtain the stellar masses and star formation rates for the SDSS-$GALEX$ sample.

While the SDSS-$GALEX$ data discussed above is derived from VAGC Data Release 7, since the release of the catalog, there have been significant improvements in the photometry. Notably, Blanton et al. (2011) find that the background subtractions in SDSS Data Release 7 has a size dependent bias in the galaxy fluxes. In addition Bernardi et al. (2013) find that the luminosity, and ultimately stellar mass, is underestimated when they are derived from the SDSS cmodel magnitudes in comparison to PyMorph single-Sérsic and Sersic-Exponential fits to the surface brightness profiles.

In order to quantify the effects of these photometric underestimations in our analysis, we replace our SDSS fluxes in the $ugriz$ band with $ugriz$ fluxes from the NASA-Sloan Atlas (NSA) catalog, which incorporate the improved background subtraction presented in Blanton et al. (2011) and uses single-Seric fit fluxes rather than the standard SDSS cmodel fluxes. Using the ratio of the luminosity derived from the improved photometry over the luminosity derived from the standard VAGC-VAGC photometry, we apply a preliminary correction to the stellar mass values obtained from iSEDfit assuming a consistent mass-to-light ratio. This mass correction leads to a significant increase in the stellar mass func-

[14] http://wise2.ipac.caltech.edu/docs/release/allsky

tion for $\mathcal{M} > 10^{11}\mathcal{M}_\odot$; however, the effect of the mass correction was negligible for the quiescent fraction evolution results. As a result, we do not include the mass corrections and do not discuss the issues with photometric measurements any further in this paper. The effects of the discussed photometry methods on the luminosity function and stellar mass function will be examined in detail in future work.

From the low redshift SDSS-$GALEX$ and intermediate redshift PRIMUS data, in this section, we define our mass complete galaxy sample. We begin by imposing the parent sample selection criteria from Moustakas et al. (2013). More specifically, we take the statistically complete $primary$ sample from the PRIMUS data (Coil et al. 2011) and impose magnitude limits on optical selection bands as specified in Moustakas et al. (2013) Table 1. These limits are in different optical selection bands and have distinct values for the five PRIMUS target fields. We then exclude stars and broad-line AGN to only select objects spectroscopically classified as galaxies, with high-quality spectroscopic redshifts ($Q \geq 3$). Lastly, we impose a redshift range of $0.2 < z < 0.8$ for the PRIMUS galaxy sample, where $z > 0.2$ is selected due to limitations from sample variance and $z < 0.8$ is selected due to the lack of sufficient statistics in subsamples defined below.

For the PRIMUS objects that meet the above criteria, we assign statistical weights (described in Coil et al. 2011 and Cool et al. 2013) in order to correct for targeting incompleteness and redshift failures. The statistical weight, w_i, for each galaxy is given by

$$w_i = (f_{\text{target}} \times f_{\text{collision}} \times f_{\text{success}})^{-1}, \quad (1)$$

as in Equation (1) in Moustakas et al. (2013). Since we are ultimately interested in a mass complete galaxy sample to derive SMFs and QFs, next we impose stellar mass completeness limits to our galaxy sample.

Stellar mass completeness limits for a magnitude-limited survey such as PRIMUS are functions of redshift,

TABLE 1
Galaxy Subsamples

	$n_{\rm env}$	$N_{\rm gal}$		$\mathcal{M}_{\rm lim}$		$M_{\rm r,lim}$
		Quiescent	Star-Forming	Quiescent	Star-Forming	
$0.05 < z < 0.12$	$n_{\rm env} < 0.5$	4969	5943	$10^{10.2}\mathcal{M}_\odot$	$10^{10.2}\mathcal{M}_\odot$	-20.98
	$n_{\rm env} > 3.0$	17488	12244			
	all	33968	30058			
$0.2 < z < 0.4$	$n_{\rm env} < 0.5$	282	1020	$10^{9.8}\mathcal{M}_\odot$	$10^{9.8}\mathcal{M}_\odot$	-21.10
	$n_{\rm env} > 3.0$	410	850			
	all	995	2628			
$0.4 < z < 0.6$	$n_{\rm env} < 0.5$	426	1226	$10^{10.3}\mathcal{M}_\odot$	$10^{10.3}\mathcal{M}_\odot$	-21.06
	$n_{\rm env} > 3.0$	543	983			
	all	1462	3334			
$0.6 < z < 0.8$	$n_{\rm env} < 0.5$	389	932	$10^{10.7}\mathcal{M}_\odot$	$10^{10.6}\mathcal{M}_\odot$	-20.90
	$n_{\rm env} > 3.0$	642	907			
	all	1590	2852			
Total		76887				

Notes: Number of galaxies ($N_{\rm gal}$) in the mass complete subsamples within the edges of the survey (Section 2). The subsamples are classified based on environment $n_{\rm env}$ and star formation rate (star-forming or quiescent). The lowest redshift bin is derived from SDSS; the rest are from PRIMUS. We also list the stellar mass completeness limit $\mathcal{M}_{\rm lim}$ for our sample and the r-band absolute magnitude limits $M_{\rm r,lim}$ for the Environment Defining Population.

the apparent magnitude limit of the survey, and the typical stellar mass-to-light ratio of galaxies near the flux limit. As in Moustakas et al. (2013), we follow Pozzetti et al. (2010) to empirically determine the stellar mass completeness limits. For each of the target galaxies we compute $\mathcal{M}_{\rm lim}$ using $\log \mathcal{M}_{\rm lim} = \log \mathcal{M} + 0.4(m - m_{\rm lim})$, where $\mathcal{M}$ is the stellar mass of the galaxy in $\mathcal{M}_\odot$, $\mathcal{M}_{\rm lim}$ is the stellar mass of each galaxy if its magnitude was equal to the survey magnitude limit, m is the observed apparent magnitude in the selection band, and $m_{\rm lim}$ is the magnitude limit for our five fields. We construct a cumulative distribution of $\mathcal{M}_{\rm lim}$ for the 15% faintest galaxies in $\Delta z = 0.04$ bins. In each of these redshift bins, we calculate the minimum stellar mass that includes 95% of the galaxies. Separately for quiescent and star-forming galaxies, we fit quadratic polynomials to the minimum stellar masses versus redshift (star-forming or quiescent classification is described in the following section). Finally, we use the polynomials to obtain the minimum stellar masses at the center of redshift bins, $0.2 - 0.4$, $0.4 - 0.6$, and $0.6 - 0.8$, which are then used as PRIMUS stellar mass completeness limits.

For the low redshift portion of our galaxy sample, we start by limiting the SDSS-$GALEX$ data to objects within $0.05 < z < 0.12$, a redshift range later imposed on the volume-limited Environment Defining Population (Section 2.5). To account for the targeting incompleteness of the SDSS-$GALEX$ sample, we use the statistical weight estimates provided by the NYU-VAGC catalog. Furthermore, we determine a uniform stellar mass completeness limit of $10^{10.2}\mathcal{M}_\odot$ above the stellar mass-to-light ratio of the SDSS-$GALEX$ data within the imposed redshift limits. We then apply this mass limit in order to obtain our mass-complete galaxy sample at low redshift.

We now have a stellar mass complete sample derived from SDSS-$GALEX$ and PRIMUS data. Since our sample is derived from two different surveys, we account for the disparity in the redshift uncertainty. While PRIMUS provides a large number of redshifts out to $z = 1$, due

to using a prism instead of a grating, the uncertainties are significantly larger ($\sigma_z/(1 + z) \approx 0.5\%$) than that of the SDSS-$GALEX$ redshifts. In order to have comparable environment measures throughout our redshift range, we apply PRIMUS redshift uncertainties to our galaxy sample selected from SDSS-$GALEX$. For each SDSS-$GALEX$ galaxy, we adjust its redshift by randomly sampling a Gaussian distribution with standard deviation $\sigma = 0.005(1 + z_{\rm SDSS-GALEX})$, where $z_{\rm SDSS-GALEX}$ is the redshift of the galaxy.

We present the absolute magnitude (M_r) versus redshift for the galaxy sample (black squares) in Figure 1. The left-most panel corresponds to the sample derived from the SDSS-$GALEX$ data and the rest correspond to the target sample derived from the PRIMUS data divided in bins with $\Delta z \sim 0.2$.

2.3. Classifying Quiescent and Star-Forming Galaxies

We now classify our mass complete galaxy sample into quiescent or star-forming using an evolving cut based on specific star-formation rate utilized in Moustakas et al. (2013) Section 3.2. This classification method uses the star-forming (SF) sequence, which is the correlation between star-formation rate (SFR) and stellar mass in star-forming galaxies observed at least until $z \sim 2$ (Noeske et al. 2007). The PRIMUS sample displays a well-defined SF sequence within the redshift range of our galaxy sample. Using the power-law slope for the SF sequence from Salim et al. (2007) (SFR $\propto \mathcal{M}^{0.65}$) and the minimum of the quiescent/star-forming bimodality, determined empirically, we obtain the following equation to classify the target galaxies (Equation 2 in Moustakas et al. 2013):

$$\log(\text{SFR}_{\rm min}) = -0.49 + 0.64\log(\mathcal{M} - 10) + 1.07(z - 0.1), \tag{2}$$

where $\mathcal{M}$ is the stellar mass of the galaxy. If the target galaxy SFR and stellar mass lie above Equation 2.3 we classify it as star-forming; if below, as quiescent (Moustakas et al. 2013 Figure 1.).

2.4. *Galaxy Sample*

2.5. *Galaxy Environment*

We define the environment of a galaxy as the number of neighboring Environment Defining Population galaxies (defined below) within a fixed aperture centered around it. We use a fixed aperture measurement of environment in order to probe environment on the halo scale, as Muldrew et al. (2012) finds in their comparison of different environment definition using simulations.

For our aperture, we use a cylinder of dimensions: $R_{\rm ap} = 2.9{\rm Mpc}$ and $H_{\rm ap} = 36{\rm Mpc}$. Though spherical apertures are often used in literature (e.g. Croton et al. 2005), we use a cylindrical aperture in order to account for the PRIMUS redshift errors and redshift space distortions (i.e. "Finger of God" effect). Cooper et al. (2005) finds that ± 1000 km s^{-1} optimally reduces the effects of redshift space distortions. The PRIMUS redshift uncertainty at $z \sim 0.7$ corresponds to $\sigma_z < 0.01$, so our aperture height choice of 36 Mpc accounts for both of these effects. Our choice of cylinder radius was motivated by scale dependence analyses in literature (Blanton et al. 2006; Wilman et al. 2010; Muldrew et al. 2012), which suggest that galactic properties such as color and quenched fractions are dependent on halo-scale properties such as host dark matter halo mass. Wilman et al. (2010), which uses environment defined by annuli of different radii, find positive correlation for quenched fraction and color on scales < 1 Mpc. Our choice of 2.9Mpc provides sufficient sample size of galaxies in dense environments, for robust statistics, while tracing galactic properties within the halo scale.

Before we measure the environment for our galaxy sample, we first construct a volume limited Environment Defining Population (EDP) with absolute magnitude cut-offs (M_r) at redshift bin of $\Delta z \sim 0.2$. The M_r cut-offs for the EDP are selected such that the cumulative number density over M_r for all redshift bins are equal. In addition to providing a reasonable comparison of environment measurements for wide redshift range, we make this choice in order to construct an EDP that contains similar galaxy populations through the redshift range (i.e. accounts for the progenitor bias). As Behroozi et al. (2013) and Leja et al. (2013) find in their analysis of the cumulative number density method, though it does not precisely account for the scatter in mass accretion or galaxy-galaxy mergers, it provides a reasonable means to compare galaxy populations over a wide range of cosmic time.

In constructing the EDP for the PRIMUS (hereafter PRIMUS EDP) we use the same PRIMUS data used to select our galaxy sample (described in Section 2.4). We again restrict the PRIMUS galaxies to $0.2 < z < 0.8$ and divide them into bins of $\Delta z = 0.2$. Before we consider the cumulative number densities in the redshift bins, we first determine the M_r limit for the highest redshift bin ($0.6 - 0.8$) by examining the M_r distribution with bin size $\Delta M_r = 0.25$ and select $M_{r,\rm lim}$ near the peak of the distribution where bins with $M_r > M_{r,\rm lim}$ have fewer galaxies than the bin at $M_{r,\rm lim}$. We conservatively choose $M_{r,\rm lim}(0.6 < z < 0.8)$ to be $M_r = -20.98$. Then for the lower redshift bins, we impose absolute magnitude limits ($M_{r,\rm lim}$) such that the cumulative number density, calculated with the galaxy statistical weights, of the bin ordered by M_r is equal to the cumulative number density of the highest redshift bin at $M_{r,\rm lim}(0.6 < z < 0.8) = -20.98$.

For the EDP of the SDSS-*GALEX* galaxy sample (hereafter SDSS EDP), we do not use the SDSS-*GALEX* parent data, which uses the geometry of the combined angular selection function of the VAGC and *GALEX* (Section 2.2). Instead, since FUV, NUV values are not necessary for the EDP, we extend the parent data of the SDSS EDP to the entire NYU VAGC, including galaxies outside of the *GALEX* window function. Furthermore, we impose a redshift range of $0.05 - 0.12$ on the SDSS EDP. This redshift range was determined to account for the lack of faint galaxies at $z \sim 0.2$ and the lack of bright galaxies at $z \sim 0.01$ in the VAGC. As with the PRIMUS redshift bins, we determine the SDSS EDP $M_{r,\rm lim}$ by matching the cumulative number density of the highest redshift bin. For redshift bins $0.05 - 0.12$, $0.2 - 0.4$, $0.4 - 0.6$, $0.6 - 0.8$ we get $M_{r,\rm lim} = -20.90$, -21.06, -21.10 and -20.98, respectively. These absolute magnitude limits are illustrated in Figure 1, which show clear M_r cutoffs in the M_r distribution versus redshift for the EDP (red circles) on top of the target galaxy sample (black).

For our SDSS-*GALEX* galaxy sample, in Section 2.4, we apply PRIMUS redshift errors in order to establish a consistent measurement of environment throughout our redshift range. We appropriately apply equivalent redshift adjustments for the SDSS EDP. So for the SDSS EDP galaxies that are within the SDSS-*GALEX* sample, we adjust the redshift by an identical amount. For the rest, we apply the same redshift adjustment procedure described in Section 2.4 in order to obtain PRIMUS level redshift uncertainties.

Finally we measure the environment for each galaxy in our galaxy sample by counting the number of EDP galaxies, $n_{\rm env}$ with *RA*, *Dec*, and z within our cylindrical aperture centered around it. $n_{\rm env}$ accounts for the statistical weights of the EDP galaxies. Once we obtain environment measurements for all the galaxies in our galaxy sample, we classify galaxies with $n_{\rm env} < 0.5$ to be "low" environment density and galaxies with $n_{\rm env} > 3$ to be "high" environment densities. The high environment cutoff was selected in order to reduce contamination from galaxies in low environment densities while maintaining sufficient statistics.

The analysis we describe below uses a fixed cylindrical aperture with dimensions $R_{\rm ap} = 2.9$ Mpc and $H_{\rm ap} = 36$ Mpc to measure environment. The same analysis was extended for varying aperture dimensions $R_{\rm ap} = 1.4, 2.9, 4.3$ Mpc and $H_{\rm ap} = 36, 71$ Mpc. We also adjusted the environment classification thresholds for these analyses. The results obtained from using different apertures and environment classification thresholds are qualitatively consistent with the results presented below.

2.6. *Edge Effects*

One of the challenges in obtaining accurate galaxy environments using a fixed aperture method is accounting for the edges of the survey. For galaxies located near the edge of the survey, part of the fixed aperture encompassing it will lie outside the survey regions. In this case, n_{env} only reflects the fraction of the environment within
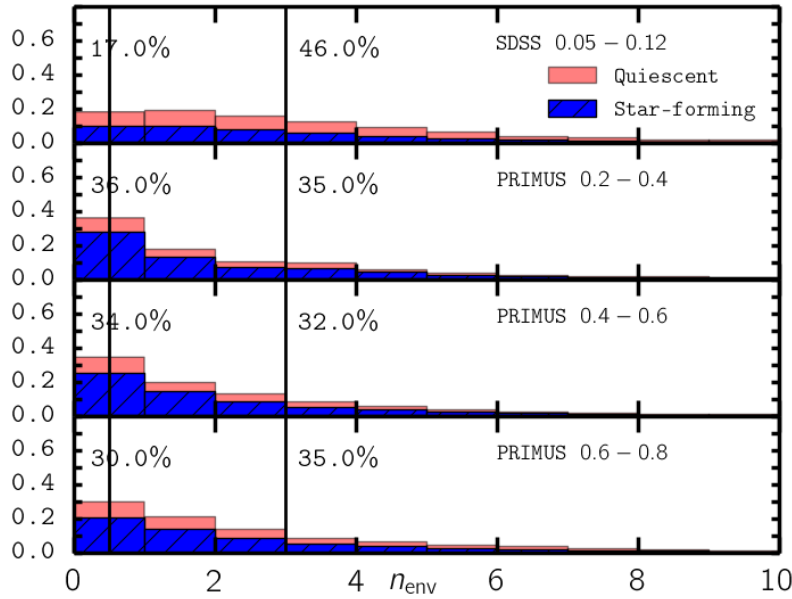
FIG. 2.— Normalized distribution of environment measurements ($n_{\rm env}$) for our mass complete galaxy sample within the edges. The star-forming galaxies contribution to the distribution is colored blue and diagonally patterned. The contribution from quiescent galaxies is colored in red. Each redshift panel is divided into three sections of by the environment classification cutoffs (vertical black lines): low density environment $n_{\rm env} < 0.5$ and high density environment $n_{\rm env} > 3.0$. The percentages of the redshift bin contained in the environment classifications are presented above the distribution. For example at $0.2 < z < 0.4$, 56.0% of galaxies in the redshift bin have low density environments while 29.0% of galaxies in the redshift bin have high density environments.

the survey geometry.

To account for these edge effects, we use a Monte Carlo method to impose edge cutoffs on our galaxy sample. First, using `ransack` from Swanson et al. (2008), we construct a random sample of $N_{\rm ransack} = 1,000,000$ points with RA and Dec randomly selected within the window function of the EDP (SDSS EDP and PRIMUS EDP separately). We then compute the angular separation, $\theta_{i,\rm ap}$ that corresponds to $R_{\rm ap}$ (Section 2.5) at the redshift of each sample galaxy i. For each sample galaxy we count the number of `ransack` points within $\theta_{i,\rm ap}$ of the galaxy: $n_{i,\rm ransack}$. Afterwards, we compare $n_{i,\rm ransack}$ to the expected value computed from the angular area of the environment defining aperture and the EDP window function:

$$< n_{\rm ransack} >_i = \frac{N_{\rm ransack}}{A_{\rm EDP}} \times \pi \theta_{i,\rm ap}^2 \times f_{\rm thresh}. \quad (3)$$

$A_{\rm EDP}$ is the total angular area of the EDP window function and $f_{\rm thresh}$ is the fractional threshold for the edge effect cut-off. For $R_{\rm ap} = 2.9$ Mpc, $f_{\rm thresh} = 0.75$. If $n_{i,\rm ransack}$ is greater than $< n_{\rm ransack} >_i$ then galaxy i remains in our sample; otherwise, it is discarded.

Once the edge effect cuts are applied, we are left with the final galaxy sample. In Figure 2 we present the distribution of environment measurements ($n_{\rm env}$) for our final galaxy sample in redshift bins: $0.05 - 0.12$, $0.2 - 0.4$, $0.4 - 0.6$, and $0.6 - 0.8$. The quiescent galaxy contributions are colored in red while the star-forming galaxy contributions are colored in blue and patterned. The low and high density environment classifications are represented by black vertical lines that divide the distribution at $n_{\rm env} = 1.5$ and $n_{\rm env} = 3.5$. The percentage of the total

galaxies in the redshift bin that are in these environment densities are labeled on the figure.

Although we imposed PRIMUS redshift errors on our SDSS galaxies in order to consistently measure environment throughout our entire sample, we note a significant discrepancy between the SDSS and PRIMUS samples in the fractional contribution of each environment classification within the redshift bin. For each of the PRIMUS redshift bins, approximately 50% of galaxies in the redshift bin are in low density environments and roughly 30% are in high density environments. In contrast, in the SDSS redshift bin, 38% of galaxies in the redshift bin are in low density environments and 45% are in high density environments. We remind the reader that this is due to the different mass-completeness limits imposed on our galaxy sample for each redshift bins.

3. STELLAR MASS FUNCTION

Our galaxy sample has so far been classified into quiescent or star-forming and low or high density environments. We further divide these subsamples into redshift bins: $0.05 - 0.12$, $0.2 - 0.4$, $0.4 - 0.6$, and $0.6 - 0.8$ for a total 16 subsamples. In Section 3.1, we calculate the SMF for each of these subsamples. Then we examine the evolution of active and quiescent subsample SMFs in different environments in Section 3.2.

3.1. *Stellar Mass Function Calculations*

To calculate the SMFs we employ a non-parametric $1/V_{\rm max}$ estimator commonly used for galaxy luminosity functions and stellar mass functions, as done in Moustakas et al. (2013) and discussed in the review Johnston (2011). The differential SMF is given by the following
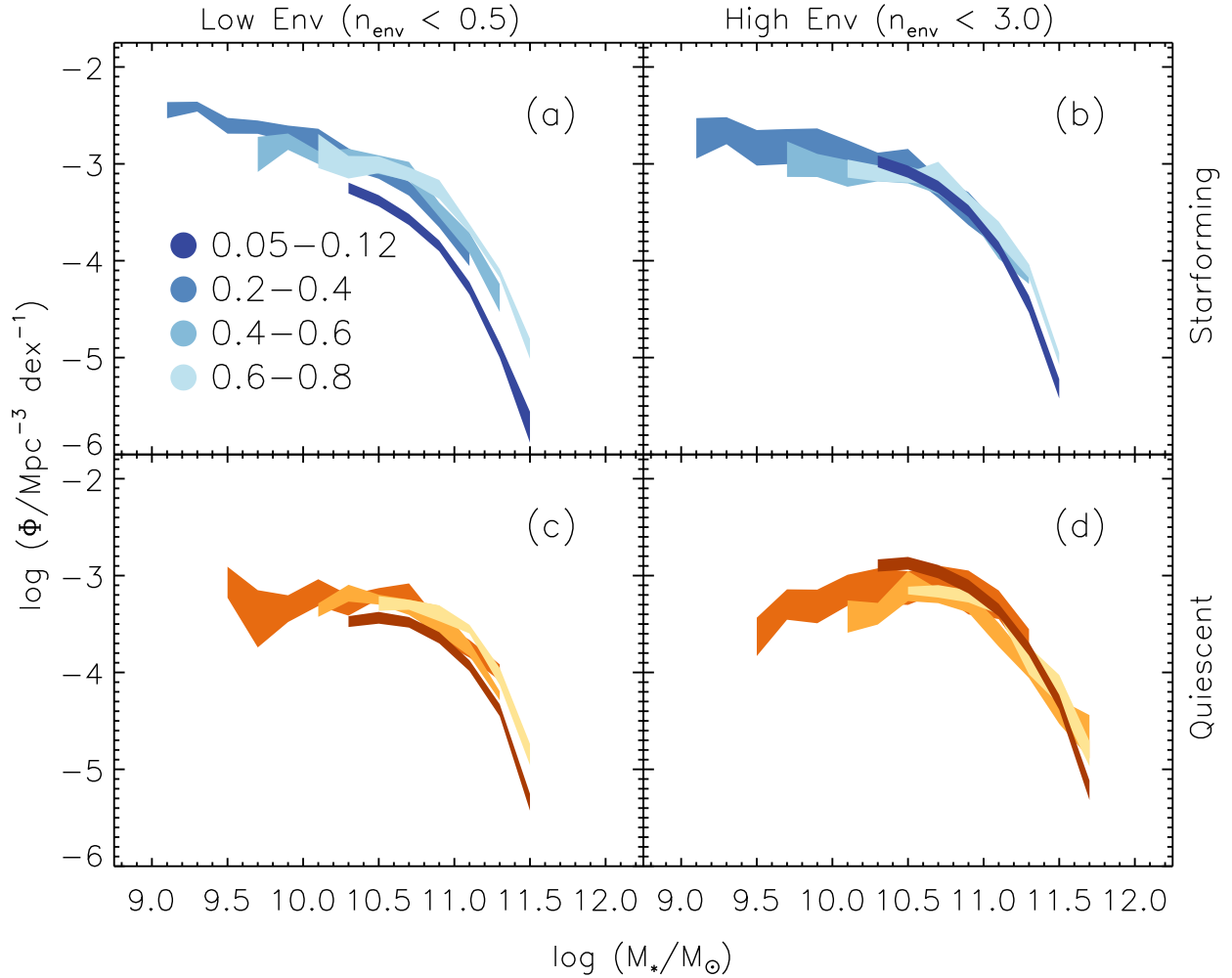
FIG. 3.— Evolution of stellar mass functions of star-forming (top) and quiescent (bottom) target galaxies in low (left) and high (right) environments from redshift range $z = 0 - 0.8$. The environment of each galaxy was calculated using a cylindrical aperture size of $R = 2.9$ Mpc and $H = 36$ Mpc and classification based on the cut-offs specified in Table ??. The SMFs use mass bins of width $\Delta \log(\mathcal{M}/\mathcal{M}_\odot) = 0.25$. In each panel we use shades of blue (star-forming) and orange (quiescent) to represent the SMF at different redshift, higher redshifts being progressively lighter.

equation:

$$\Phi(\log \mathcal{M})\Delta(\log \mathcal{M}) = \sum_{i=1}^{N} \frac{w_i}{V_{\text{max,avail,i}}}. \qquad (4)$$

w_i is the statistical weight of galaxy i and $\Phi(\log \mathcal{M})\Delta(\log \mathcal{M})$ is the number of galaxies (N) per unit volume within the stellar mass range $[\log \mathcal{M}, \log \mathcal{M} + \Delta(\log \mathcal{M})]$. The equation above is same as Equation 3. in Moustakas et al. (2013) except that we use $V_{\text{max,avail}}$ instead than V_{max}, to account for the edge effects of the survey discussed in Section 2.6.

$V_{\text{max,i}}$ is the maximum cosmological volume where it is possible to observe galaxy i given the apparent magnitude limits of the survey. However in Section 2.6 we remove galaxies that lie on the edge from our sample. In doing so we reduce the maximum cosmological volume where a galaxy can be observed, thereby reducing $V_{\text{max,i}}$. We introduce the term $V_{\text{max,avail,i}}$ for the $V_{\text{max,i}}$ value that accounts for the survey edge effects.

To calculate $V_{\text{max,avail,i}}$, we use a similar Monte Carlo

method as the edge effect cutoffs in Section 2.6. First, we generate a sample of points with random RA, Dec within the window function of our galaxy sample (SDSS-$GALEX$ window function and the five PRIMUS fields) and random z within the redshift range. These points are not to be confused with the ransack sample in Section 2.6. We apply the edge effect cutoffs on these random points as we did for our galaxy sample using the same ransack method in Section 2.6. At redshift bins of $\Delta z \sim 0.01$, we calculate the fraction of the random points that remain in the bin after the edge effect cutoffs over the total number of random points in the bin: f_{edge}. We then apply this factor to compute $V_{\text{max,avail}} = V_{\text{max}} \times f_{\text{edge}}$. The V_{max} in the equation above are computed following the method described in Moustakas et al. (2013) Section 4.2 with the same redshift-dependent K-correction from observed SED and luminosity evolution model.

To calculate the uncertainty of the SMFs from the sample variance, we use a standard jackknife technique (as done in Moustakas et al. 2013). For the PRIMUS galax-

ies, we calculate SMFs after excluding one of the five target fields at a time. For the SDSS target galaxies we divide the field into a 12×9 rectangular *RA* and *Dec* grid and calculate the SMFs after excluding one grid at a time. From the calculated SMFs we calculate the uncertainty:

$$\sigma^j = \sqrt{\frac{M-1}{M} \sum_{k=1}^{M} (\Phi_k^j - \langle \Phi^j \rangle)^2} \qquad (5)$$

M in this equation is the number of jack knife SMFs in the stellar mass bin. $\langle \Phi^j \rangle$ is the mean number density of galaxies in each stellar mass bin for all of the jack knife Φ^js.

3.2. *Evolution of the Stellar Mass Function in Different Environments*

In Figure 3, we present the SMFs of the quiescent/star-forming (orange/blue, bottom/top panels) and high/low density environment (left/right panels) subsamples. The redshift evolution of the SMFs in each of these panels are indicated by a darker shade for lower redshift bins. The width of the SMFs represent the sample variance uncertainties.

While a detailed comparison of the SMFs in each panel for different epochs are complicated due to the different stellar mass completeness limits, we present some notable trends in each panel. In panel (a), star-forming galaxies in low density environments, we find a significant decrease in the high mass end of the SMF ($\mathcal{M} > 10^{10.75} \mathcal{M}_\odot$). In contrast at lower masses ($\mathcal{M} < 10^{10.5} \mathcal{M}_\odot$) we observe a notable increase in the SMF. In panel (b), star-forming galaxies in high density environments, we notice a possible decrease above the knee of the SMF ($\mathcal{M} \sim 10^{10.7} \mathcal{M}_\odot$) accompanied by an increase below the knee. For the quiescent population in low density environment, shown in panel (c) of Figure 3, we notice an increase in Φ for lower masses, but we do not notice any clear SMF evolution at the massive end. Lastly for the quiescent population in high density environments, panel (d), we find significant increase in Φ at all masses.

In comparison to results from DEEP2 (Bundy et al. 2006) and zCOSMOS (Bolzonella et al. 2010), some of the noted trends are not immediately evident. However, this is mostly due to the conflicting mass limits proposed in each study. In addition, only part of the redshift range probed by Bundy et al. (2006) overlap with our results. Overall, we find that the trends we note in the SMF evolution above are in good agreement with Bundy et al. (2006) and Bolzonella et al. (2010).

Observing the evolutionary trends in SMF for each of these sub-populations provides a narrative of the different galaxy evolutionary tracks involving environment and quenching. For example, the decrease in the massive star-forming galaxies in low density environments over cosmic time can be attributed to the transition of those galaxies to any of the other panels. The star-forming galaxies in low density environments that have quenched their star formation over time are possibly responsible for the increase of the quiescent, low density environment SMF over time. The star-forming galaxies that fall into higher density environments explain the increase in the

star-forming high density environment SMF below the knee. Finally, star-forming galaxies in high density environments that have quenched their star-formation, quiescent galaxies that have transitioned from low to high density environments, and star-forming galaxies in low density environments that quench their star-formation while infalling to high density environments all contribute to the overall increase of the high environment quiescent SMF.

In addition to the evolution over cosmic time, we observe noticeable trends when we compare the SMFs for star-forming and quiescent galaxies between the two environments. Comparison of the SMFs in low versus high density environments reveal a noticeable relation between mass and density, with SMFs in high density environments having more massive galaxies. We further confirm this trend when we compare the median mass between the two environments to find that the median mass for galaxies in high density environments is significantly greater than in low density environments. The relationship between mass and environment observed in our SMFs mirror the well-established mass-density relation and observed mass segregation with environment in the literature (Bundy et al. 2006; Scodeggio et al. 2009; Bolzonella et al. 2010).

While our mass complete subsample coupled with robust environment measurement allows us to compare SMF evolution for each of our subsamples out to $z = 0.8$, we caution readers and reserve detailed analysis of the SMFs to future work due to the improvements in photometry that significantly alter the SDSS SMFs mentioned in Section 2.2.

4. QUIESCENT FRACTION

The SMFs calculated in the previous section illustrate the stellar mass distribution of our galaxy population and its evolution over cosmic time. In this section, using the SMFs of our subsamples, we compare the quiescent and the star-forming populations by calculating the fraction of galaxies that have quenched their star-formation, the quiescent fraction.

While the fractional relation of the star-forming and quiescent populations has been investigated in the past, with limited statistics, disentangling the environmental effects f rom underlying correlations among observable galaxy properties such as the color-mass or mass-density relations (Cooper et al. 2010) remains a challenge. With the sufficient statistics available from SDSS and PRIMUS, we evaluate the quiescent fraction in bins of stellar mass, redshift, and environment in Section 4.1. By analyzing the quiescent fraction with respect to these properties, in Section 4.2 we explicitly compare the quiescent fraction evolution in low and high density environments. Our comparison reveal the subtle environmental effects on the quiescent fraction evolution. Furthermore, by quantifying this environmental effect, we are able constrain the role of environmental quenching in galaxy evolution.

4.1. *Evolution of the Quiescent Fraction*

From the SMF number densities (Φ) computed in the previous section, the quiescent fraction is computed as

FIG. 4.— Evolution of the quiescent fraction f_Q for galaxies in low (left) and high (rights) density environments for $z < 0.8$. f_Qs were calculated using the SMFs in Figure3, as described in text. Darker shading indicates lower redshift and the width represents the standard jackknife uncertainty.

follows,

$$f_Q = \frac{\Phi_Q}{\Phi_{SF} + \Phi_Q}. \qquad (6)$$

Φ_Q and Φ_{SF} are the total number of galaxies per unit volume in stellar mass bin of $\Delta(\log \mathcal{M}) = 0.20$ dex for the quiescent and star-forming subsamples, respectively (Equation 4). We compute f_Q for high and low density environments for all redshift bins as plotted in Figure 4, which shows the evolution of f_Q for high (right panel) and low (left panel) density environments. As in Figure 3, the evolution of the quiescent fraction over cosmic time is represented in the shading (darker with lower redshift) and the uncertainty is represented by the width. For the uncertainty in the quiescent fraction, we use the standard jackknife technique, following the same steps as the SMF uncertainty in Section 3.1.

Most noticeably in Figure 4, we find f_Q increases monotonically as a function of mass at all redshift bin and environment. In other words, for all subsamples, galaxies in higher mass bins are more likely to have quenched its star-formation. With the roughly linear correlation between galaxy SFR to galaxy color and morphology, we find that this trend reflects the well established color-mass and morphology-mass relations: more massive galaxies are more likely to be red or early-type (Blanton & Moustakas 2009).

Focusing on the redshift evolution of f_Q, we find that for both environments f_Q increases as redshift decreases. For high density environments, this is analogous to the Butcher-Oemler Effect (Butcher & Oemler 1984), which states that galaxy populations in groups or clusters have higher $f_{\rm blue}$, or lower f_Q, at higher redshift. For all environments, a larger portion of our galaxy population has quenched its star-formation over time. Coupled with the decline of SFR in the star-forming population (Noeske et al. 2007; Cooper et al. 2008), our results are in agreement with the observed decline of global star-formation in the universe (Hopkins & Beacom 2006).

In addition, when we compare the stellar masses at which $f_Q = 0.5$ for each subsample, the so-called $\mathcal{M}_{50-50}$, we find that this quantity decreases over cosmic time. This corresponds to the well-known mass-downsizing pattern in the literature (e.g. Bundy et al. 2006). Furthermore, the mass-downsizing trend observed in each of our environment subsample is consistent with the trend observed in zCOSMOS Redshift Survey for isolated and group galaxies (Iovino et al. 2010).

Finally, we compare between our low and high density environment f_Qs at each redshift bin interval. For our lowest redshift bin, we find that f_Q at low density environments ranges from ~ 0.4 to ~ 0.8 for $10^{10.2}\mathcal{M}_\odot < \mathcal{M}_* < 10^{11.5}\mathcal{M}_\odot$. Over the same mass range, f_Q at high density environment ranges from ~ 0.55 to ~ 0.9. Evidently for our SDSS sample, f_Q in high density environment is notably higher.

For our PRIMUS sample at $z \sim 0.3$, over $10^{9.5}\mathcal{M}_\odot < \mathcal{M}_* < 10^{11}\mathcal{M}_\odot$ f_Q ranges from ~ 0.15 to ~ 0.55 for low density environment, while at high density environment f_Q ranges from ~ 0.2 to ~ 0.7. Similarly, at $z \sim 0.5$, over $10^{10}\mathcal{M}_\odot < \mathcal{M}_* < 10^{11.2}\mathcal{M}_\odot$ f_Q ranges from ~ 0.25 to ~ 0.55 for low density environment and f_Q ranges from ~ 0.3 to ~ 0.7. Finally in our highest redshift bin $z \sim 0.7$, over the mass range $10^{10.5}\mathcal{M}_\odot < \mathcal{M}_* < 10^{11.5}\mathcal{M}_\odot$, f_Q ranges from ~ 0.3 to ~ 0.55 for low density and ~ 0.45 to ~ 0.8 for high density. For the entire redshift range of our sample, f_Q in high density environment is higher than f_Q in low density environments.

While there is a significant difference in f_Q between the environments, since the difference is observed from our highest redshift bin it is not necessarily a result of environment dependent quenching mechanisms. In order to isolate the environmental dependence on star-formation quenching, in the following section we quantitatively compare the evolution of the quiescent fraction between the different environments.
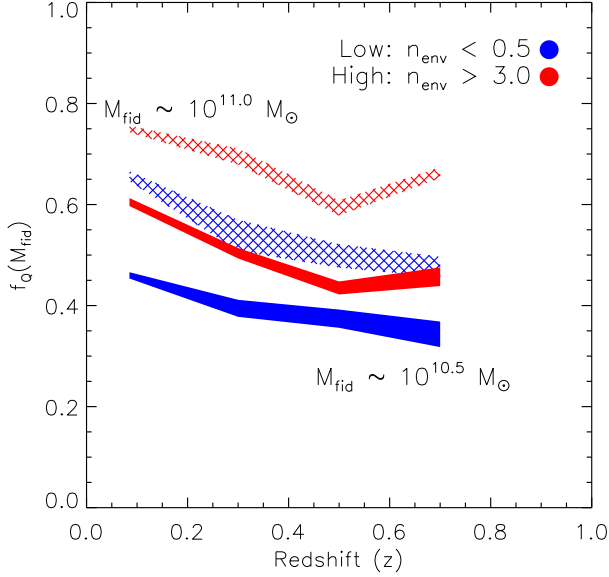
FIG. 5.— The evolution of the quiescent fraction at fiducial mass, $f_Q(\mathcal{M}_{\rm fid})$, for low (blue) and high (red) density environments within the redshift range $z = 0.0 - 0.8$. We present the $f_Q(\mathcal{M}_{\rm fid})$ evolution for $\mathcal{M}_{\rm fid} = 10^{10.5}\mathcal{M}_\odot$ (solid fill) and $10^{11}\mathcal{M}_\odot$ (patterned fill) with the uncertainty of the best-fit parameter b in Equation 7 represented by the width of the evolution. While the high density $f_Q(\mathcal{M}_{\rm fid})$ is greater than low density environment $f_Q(\mathcal{M}_{\rm fid})$ over the entire redshift range of our sample, there is a significant increase in $f_Q(\mathcal{M}_{\rm fid})$ over cosmic time for both environments. For the environment cut-offs ($n_{\rm env} < 0.5$ for low and $n_{\rm env} > 3.0$ for high), there is no significant difference in the slope of the evolution between the environments.

TABLE 2
BEST FIT PARAMETERS FOR $f_Q(\mathcal{M}_*)$ FIT

$z_1 < z < z_2$	Environment	a	b
$0.05 < z < 0.12$	$n_{\rm env} < 0.5$	0.392 ± 0.020	0.482 ± 0.006
	$n_{\rm env} > 3.0$	0.289 ± 0.015	0.605 ± 0.008
$0.2 < z < 0.4$	$n_{\rm env} < 0.5$	0.289 ± 0.039	0.395 ± 0.016
	$n_{\rm env} > 3.0$	0.383 ± 0.016	0.504 ± 0.010
$0.4 < z < 0.6$	$n_{\rm env} < 0.5$	0.248 ± 0.042	0.374 ± 0.018
	$n_{\rm env} > 3.0$	0.317 ± 0.034	0.435 ± 0.013
$0.6 < z < 0.8$	$n_{\rm env} < 0.5$	0.267 ± 0.058	0.343 ± 0.025
	$n_{\rm env} > 3.0$	0.412 ± 0.023	0.457 ± 0.018

Notes: Best fit parameters in Equation 7 for each subsample $f_Q(\mathcal{M}_*)$ in Figure 4 for $\mathcal{M}_{\rm fid} = 10^{10.5}\mathcal{M}_\odot$.

4.2. Environmental Effects on the Quiescent Fraction Evolution

In order to more quantitatively compare the f_Q evolution for different epochs and environments, we fit f_Q for each subsample to a power-law parameterization as a function of stellar mass,

$$f_Q(\mathcal{M}_*) = a \log \left(\frac{\mathcal{M}_*}{\mathcal{M}_{\rm fid}} \right) + b, \qquad (7)$$

where a and b are best-fit parameters using *MPFIT* (Markwardt 2009) and $\mathcal{M}_{\rm fid}$ represents the empirically selected fiducial mass within the stellar mass limits where there is a sufficiently large number of galaxies. We primarily focus on $\mathcal{M}_{\rm fid} = 10^{10.5}\mathcal{M}_\odot$.

In Figure 5 we present the evolution of $f_Q(\mathcal{M}_{\rm fid})$ from $z \sim 0.7$ to ~ 0.1 at low (blue) and high (red) density environments for $\mathcal{M}_{\rm fid} = 10^{10.5}\mathcal{M}_\odot$ (solid fill) and $10^{11}\mathcal{M}_\odot$ (pattern fill). The width of the evolution represents the uncertainty derived from *MPFIT*. As noted earlier in Section 4.1, f_Q in high density environment is significantly greater than f_Q in low density environment for both fiducial mass choices. Throughout our sample's redshift range $f_Q(\mathcal{M}_{\rm fid})_{\rm high} - f_Q(\mathcal{M}_{\rm fid})_{\rm low} \sim 0.1$

In addition, the $f_Q(\mathcal{M}_{\rm fid})$ evolution illustrates that the quiescent fraction in low density environment increases over cosmic time: $f_Q(\mathcal{M}_{\rm fid}, z \sim 0.1) - f_Q(\mathcal{M}_{\rm fid}, z \sim 0.7) \sim 0.1$. This significant quiescent fraction evolution for low density environment suggests that internal mechanisms, independent of environment, are responsible for a significant amount of star-formation quenching. Meanwhile, the $f_Q(\mathcal{M}_{\rm fid})$ evolution in high density environment ($f_Q(\mathcal{M}_{\rm fid}, z \sim 0.1) - f_Q(\mathcal{M}_{\rm fid}, z \sim 0.7) \sim 0.12$) shows little additional evolution.

When we increase our choice of $\mathcal{M}_{\rm fid}$ to $10^{11}\mathcal{M}_\odot$, aside from an overall shift in $f_Q(\mathcal{M}_{\rm fid})$ by ~ 0.2, we observe the same evolutionary trends. $f_Q(\mathcal{M}_{\rm fid} = 10^{11}\mathcal{M}_\odot)$ for both low and high density environments each increase by ~ 0.1 from $z \sim 0.7$ to ~ 0.1. Evidently, increasing the fiducial mass to $10^{11}\mathcal{M}_\odot$ does not significantly alter the evolutionary trends in either environments. Although the varying stellar mass completeness at each redshift bin limits the masses we probe for the f_Q evolution, our f_Q evolution exhibits little mass dependence.

Considering that our fixed aperture definition of environment is susceptible to contamination due to PRIMUS redshift errors, in Figure 6, we impose more stringent high density environment classifications, extending the cut off to $n_{\rm env} > 6$ and 9 (specified in the top right legend and represented by the color of the shading). Aside from the increase in uncertainties that accompany a decrease in sample size from a purer high environment sample, we find an extension of the f_Q difference between the environments we stated earlier. A more stringent high environment classification significantly increases the overall $f_Q(\mathcal{M}_{\rm fid})$: $f_{Q, n_{\rm env}>9} > f_{Q, n_{\rm env}>6} > f_{Q, n_{\rm env}>3} > f_{Q, n_{\rm env}<0.5}$.

More importantly, a purer high environment classification reveals a more significant environment dependence on the f_Q evolution. While the difference between the f_Q evolution in low and high density environment is negligible for the $n_{\rm env} > 3$ cut-off, there is a notable difference in f_Q evolution between our highest cut-off $n_{\rm env} > 9$ and our low density environment. $f_Q(\mathcal{M}_{\rm fid}, z \sim 0.1) - f_Q(\mathcal{M}_{\rm fid}, z \sim 0.7) \sim 0.2$ for $n_{\rm env} > 9$ versus $f_Q(\mathcal{M}_{\rm fid}, z \sim 0.1) - f_Q(\mathcal{M}_{\rm fid}, z \sim 0.7) \sim 0.1$ for low density environment as we listed earlier. In addition to the environment independent internal quenching mechanisms that can explain the f_Q evolution at low density environments, there may be other environment dependent mechanisms that can account for the moderate environment dependence of the f_Q evolution. Our measured difference in the f_Q evolution between environ-
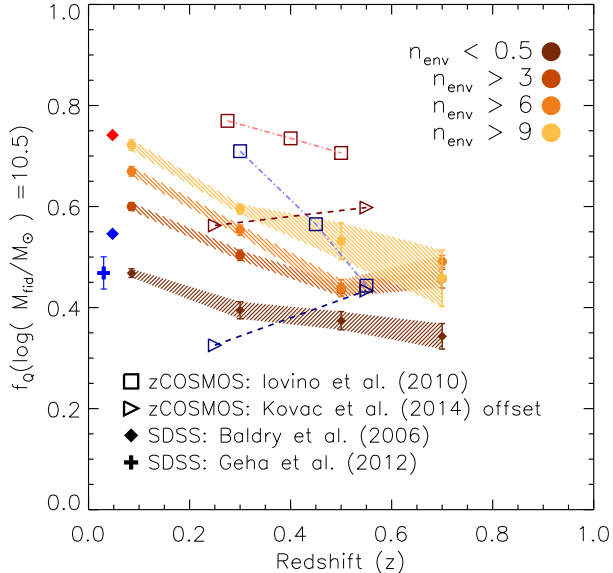
FIG. 6.— $f_Q(\mathcal{M}_{\rm fid} = 10^{10.5}\mathcal{M}_\odot)$ evolution compared to $f_{\rm red}(\mathcal{M}_* = 10^{10.5}~\mathcal{M}_\odot)$ in the literature: Iovino et al. (2010) (square) and Kovač et al. (2014) (triangle) from zCOSMOS and Baldry et al. (2006) (diamond) and Geha et al. (2012) (cross) from SDSS. The $f_{\rm red}$ values from Iovino et al. (2010), Kovač et al. (2014), and Baldry et al. (2006) are calculated from the best-fit parameterizations presented in the respective works. The f_Q value from Geha et al. (2012) is the f_Q value at $\mathcal{M} = 10^{10.55}\mathcal{M}_\odot$. High density environment is represented in red and low density environment is represented in blue. For Kovač et al. (2014) we apply the offset between the color-based and SFR-based galaxy classification in order to plot the f_Q estimates. We also plot the $f_Q(\mathcal{M}_{\rm fid} = 10^{10.5}\mathcal{M}_\odot)$ evolution of our sample with varying environment cut-offs specified on the top right. As in Figure 5 the width of the $f_Q(\mathcal{M}_{\rm fid} = 10^{10.5}\mathcal{M}_\odot)$ evolution represent the uncertainty in the best-fit parameters of Equation 7.

ments provides a strict constraint for any environmental quenching models.

4.3. Comparison to Literature

Although a direct comparison with other results is difficult due to our sample specific methodology, a number of results from literature have investigated the quiescent fraction in comparable fashions. In this section we compare our f_Q results from above to a number of these results, specifically from SDSS and zCOSMOS, with similarly defined samples and analogous environment classifications.

In Figure 6, we plot best-fit parameterization of $f_{\rm red}$ for high and low density environment from zCOSMOS, Iovino et al. (2010) (square) and Kovač et al. (2014) (triangle), and SDSS, Baldry et al. (2006) (diamond) and Geha et al. (2012) (cross). From Iovino et al. (2010) we calculate $f_{\rm red} = 1 - f_{\rm blue}$ using the best-fit $f_{\rm blue}$ from the mass bin $\mathcal{M} = 10^{10.3} - 10^{10.8}\mathcal{M}_\odot$. From Kovač et al. (2014) we plot an estimated f_Q by applying the residual between SFR based and color based galaxy classifications to the best-fit $f_{\rm red}$ at $\mathcal{M} = 10^{10.5}\mathcal{M}_\odot$ for low ($\delta = 0.0$) and high density environment ($\delta = 1.5$). Similarly, from Baldry et al. (2006) we plot f_Q derived from the best-fit $f_{\rm red}$ at $\mathcal{M} = 10^{10.5}\mathcal{M}_\odot$ for low ($\delta = 0.0$) and high density environment ($\delta = 1.0$). For Geha et al. (2012), we plot f_Q

in their mass bin closest to $10^{10.5}\mathcal{M}_\odot$, $\mathcal{M} = 10^{10.55}\mathcal{M}_\odot$.

For our lowest redshift bin SDSS sample, we find that our f_Q for low and high environments are consistent with other SDSS f_Q (or $f_{\rm red}$) measurements as a function of environment. For example, Baldry et al. (2006) uses project neighbor density environment measures (log Σ) to obtain $f_Q(\mathcal{M})$ for a range of environmental densities. Although the different environment measurements make direct comparisons unclear, in their corresponding higher environments (log $\Sigma > 0.2$ in Baldry et al. 2006) $f_Q(\mathcal{M} \sim 10^{10.2}\mathcal{M}_\odot) \sim 0.6$ and $f_Q(\mathcal{M} \sim 10^{11.5}\mathcal{M}_\odot) \sim 0.9$, which is in agreement with our high density environment. Likewise, for lower environments (log $\Sigma < -0.4$ in Baldry et al. 2006) $f_Q(\mathcal{M} \sim 10^{10.2}\mathcal{M}_\odot) \sim 0.4$ and $f_Q(\mathcal{M} \sim 10^{11.5}\mathcal{M}_\odot) \sim 0.8$, which also agree with our low density environment f_Q. The Baldry et al. (2006) points (diamond) in Figure 6 reflect this agreement.

More recently, Tinker et al. (2011), using a group-finding algorithm on the SDSS DR7, presents the relationship between f_Q and overdensity for galaxies within the mass range log $\mathcal{M} = [9.8, 10.1]$. The Tinker et al. (2011) f_Q at the lowest and highest overdensities, $f_Q \sim 0.4$ and $f_Q \sim 0.6$ respectively, are consistent with our f_Q for low and high density environment at the lower mass limit (log $\mathcal{M} \sim 10.2$).

A modified Tinker et al. (2011) sample is used in Geha et al. (2012) to obtain f_Q for isolated galaxies over a wider mass range ($10^{7.4}\mathcal{M}_\odot$ to $10^{11.2}\mathcal{M}_\odot$). Provided that Geha et al. (2012) probe a slightly lower redshift range ($z \leq 0.06$), Geha et al. (2012) present a consistent f_Q range as our SDSS f_Q. Within the overlapping mass range, at the low mass end Geha et al. (2012) find $f_Q(\mathcal{M}_* \sim 10^{10.2}\mathcal{M}_\odot) \sim 0.3$ and at the high mass end they find $f_Q(\mathcal{M}_* \sim 10^{11.2}\mathcal{M}_\odot) \sim 0.8$. Both of these values agree with our lowest redshift f_Q results in low density environment. Figure 6 illustrates the f_Q agreement for $\mathcal{M}_* = 10^{10.5}\mathcal{M}_\odot$.

For $z > 0.2$, we compare our PRIMUS f_Q results to the $f_{\rm red}$ (or $1 - f_{\rm blue}$) results from the zCOSMOS Redshift Survey (Iovino et al. 2010; Cucciati et al. 2010; Kovač et al. 2014), which covers a similar redshift range as PRIMUS. Iovino et al. (2010), Cucciati et al. (2010), and Kovač et al. (2014) using a mass-complete galaxy sample derived from zCOSMOS and a group catalog, 3D local density contrast, and overdensity environment measurements, respectively, compare $f_{\rm red}$ with respect to environment. The $f_{\rm blue}$ for group and isolated galaxies from Iovino et al. (2010) are generally inconsistent with our $1 - f_Q$ for high and low density environments.

Similarly, $f_{\rm red}$ for high and low overdensities in Kovač et al. (2014) are greater overall than the PRIMUS f_Q values in high and low density environments. However, Kovač et al. (2014) points out that there is a significant difference between classifying the quenched population using color and SFR. For their lower redshift bin ($0.1 < z < 0.4$) they find that their f_Q defined by color is greater than f_Q defined by SFR by roughly 0.2. While for their higher redshift bin ($0.4 < z < 0.7$) they find a difference of $0.15 - 0.19$. Although Kovač et al. (2014) does not elaborate on how the galaxy classification discrepancy applies to the different environments, if we simply account for the difference uniformly for $f_{\rm red}$ at all environments, the Kovač et al. (2014) results in their

lower redshift bin are roughly consistent with our f_Q at high and low density environments. However, in their higher redshift bin even accounting for the difference in galaxy classification, Kovač et al. (2014) finds a significantly higher f_Q.

In Figure 4, observing the f_Q evolution with respect mass reveal, qualitatively, little mass dependence in the evolution. Moreover, in Figure 5, we illustrated that adjusting the fiducial mass only shifted the overall $f_Q(\mathcal{M}_{\rm fid})$, but did change the f_Q evolutionary trend. The consistency in the f_Q evolutionary trends when the fiducial mass is changed suggest that f_Q evolution exhibit little mass dependence. In contrast to the weak mass dependence we observe in our results, Iovino et al. (2010) find significantly different f_Q evolutions at $\mathcal{M} \sim 10^{11}\mathcal{M}_\odot$ and $\mathcal{M} \sim 10^{10.5}\mathcal{M}_\odot$, for both group and isolated galaxies. In fact at their highest mass bin ($10^{10.9} - 10^{11.4}\mathcal{M}_\odot$), Iovino et al. (2010) find no evolution for both environments: constant $f_{\rm blue} \sim 0.1$ over $z = 0.3 - 0.8$ for both group and isolated galaxy populations.

Meanwhile in their mass bin most comparable to $\mathcal{M}_{\rm fid} \sim 10^{10.5}\mathcal{M}_\odot$ ($10^{10.3}\mathcal{M}_\odot - 10^{10.8}\mathcal{M}_\odot$), Iovino et al. (2010) finds that $f_{\rm blue}$ evolves by ~ 0.1 from $z = 0.5$ to 0.25 for group galaxies and by ~ 0.3 from $z = 0.55$ to 0.3 for isolated galaxies as presented in Figure 6. Altogether, with mass bins beyond the fiducial masses we explore, Iovino et al. (2010) find a strong mass dependence with f_Q evolving significantly more in lower mass bins. While our sample from PRIMUS provides larger statistics than zCOSMOS, the mass-completeness limits we impose on our sample limits the mass range we probe (e.g. $\mathcal{M} > 10^{10.5}\mathcal{M}_\odot$ for our $z \sim 0.7$ bin). Consequently our results cannot dismiss mass dependence in the f_Q evolution at lower masses.

In Figure 5 and Figure 6 we quantified that throughout our redshift range, high density environment has a significantly greater $f_Q(\mathcal{M}_{\rm fid})$ than the low density environment. Our findings are in agreement with the zCOSMOS results from Cucciati et al. (2010) and Kovač et al. (2014). As illustrated in Figure 6, both Cucciati et al. (2010) and Kovač et al. (2014) find f_Q in high density environment significantly greater than f_Q at low density environment. Moreover, since galaxy color serves as a proxy for SFR, our results support the existence of the color-density relation (Cucciati et al. 2010; Cooper et al. 2010) and debunks the suggestion that the color-density relation is merely a reflection of the mass-density as Scodeggio et al. (2009) suggests for $0.2 < z < 1.4$ in the Vimos VLT Deep Survey.

In Section 4.2, we pointed out that f_Q in low density environment evolved over cosmic time. From this trend we deduce that internal, environment independent, quenching mechanisms contribute to star-formation quenching in galaxy evolution. Iovino et al. (2010) from zCOSMOS, plotted in Figure 6, also find that f_Q in low density environment increases over decrease in redshift. On the other hand Kovač et al. (2014), also from zCOSMOS, presents that f_Q in low density environment decreases over cosmic time. This disagreement persists even when we account for the galaxy classification discrepancies in Figure 6.

Furthermore, in Section 4.2, our comparison of the f_Q evolution between the lowest density environment and the highest density environment revealed a modicum of evidence for the existence of environment dependent quenching mechanisms. The same comparison on zCOSMOS results (Iovino et al. 2010; Kovač et al. 2014) present trends inconsistent with our findings. First, comparing the high (red) and low (blue) density environments for Iovino et al. (2010) in Figure 6 shows that there is indeed pronounced discrepancies between the f_Q evolution in different environments. Group galaxies in Iovino et al. (2010) have higher overall f_Q than isolated galaxies. However, unlike our results, which find a greater f_Q evolution at higher density environments, Iovino et al. (2010) finds the opposite environment dependence that there is a significantly greater f_Q evolution for isolated galaxies.

Next, Kovač et al. (2014) also find that overall f_Q in high density is greater than low density environments. Like their low density environment f_Q evolution, f_Q in high density environment decreases over cosmic time between their two redshift bins. Although the decrease in f_Q over cosmic time conflicts with our results, Kovač et al. (2014) finds a greater (less negative) f_Q evolution in high density environment over low density environment, suggesting an environment dependence that is in the same direction as our results. We note that the negative slopes of the f_Q evolution in both environments are enhanced in Figure 6 due to the galaxy classification correction we impose to the Kovač et al. (2014) results. However, even without the correction (not shown), in their best-fit f_Q results, the same evolutionary trends mentioned above are observed.

While the zCOSMOS survey provides more precise spectroscopic redshifts than PRIMUS, our sample provides a significantly larger statistics. In addition, our sample covers a larger portion of the sky. Our SDSS-$GALEX$ sample covers $2,505$ deg^2. More comparably, our PRIMUS sample covers 5.5 deg^2, which is over 3 times the sky coverage of zCOSMOS, 1.7 deg^2. With a significantly greater sky coverage our sample is less susceptible to cosmic variance.

As listed in Table 1, after our edge effect cuts and stellar mass completeness limits, our sample consists of $12,861$ galaxies from PRIMUS over $0.2 < z < 0.8$ and $64,026$ galaxies from SDSS over $0.05 < z < 0.12$. Meanwhile, Iovino et al. (2010) has 914 galaxies with $\mathcal{M} > 10^{10.3}\mathcal{M}_\odot$ over $0.1 < z < 0.6$ and 1033 galaxies with $\mathcal{M} > 10^{10.6}\mathcal{M}_\odot$ over $0.1 < z < 0.8$. But for the actual sample used to obtain the best-fit f_Q values in Figure 6 Iovino et al. (2010) has 617 galaxies. In comparison, our PRIMUS sample alone contains > 20 times the number of galaxies. While there is a considerable difference in the overall f_Q between our results and those of Iovino et al. (2010), the use of different methodologies, particularly for galaxy classification and environment measurements, make the comparisons ambiguous. On the other hand, the discrepancies in the f_Q evolutionary trends with our results may be explained by the limited statistics in the Iovino et al. (2010) sample.

The more recent Kovač et al. (2014) provides larger statistics with $2,340$ galaxies in their lower redshift bin ($0.1 < z < 0.4$) and $2,448$ galaxies in their higher redshift bin ($0.4 < z < 0.7$). Although their sample falls short

of our PRIMUS sample, which contains over two times the number of galaxies, the Kovač et al. (2014) sample provides a more stable comparison. Once their results are adjusted for the different galaxy classification, we find that their overall f_Q is more or less consistent with our overall f_Q. However, it is difficult to explain the significant discrepancies in the f_Q evolutionary trends.

5. SUMMARY AND DISCUSSION

Using a stellar mass complete galaxy sampled derived from SDSS and PRIMUS accompanied by a consistently measured galaxy environment from robust spectroscopic redshifts, we measure the stellar mass functions for star-forming and quiescent in low and high density environments over the redshift range $0.05 < z < 0.8$. From these stellar mass functions, we compare the proportion of galaxies that have quenched their star-formation within the subsamples by computing quiescent fraction for each of them. Afterwards, in order to better quantify the evolution of the quiescent fraction over cosmic time, we fit our quiescent fraction anchored at a fiducial mass. From our analyses we find the following notable results.

1. By measuring the SMF evolution for each of our subsamples, we approximately trace the evolutionary tracks our galaxy population tracing the tracks of quenching mechanisms and galaxies infalling into high density environments.

2. From the SMFs, we find that our galaxy population in high density environments, both star-forming and quiescent, have a higher median mass, thus confirming the mass density relation and mass-segregation in different environments throughout our sample's redshift range.

3. For all subsamples, f_Q increases monotonically with galaxy stellar mass showing a clear mass dependence and supporting well established color-mass and morphology mass relations.

4. f_Q increases significantly with redshift for both low and high density environments. For high density environment, this trend is the Butcher-Oemler effect. Furthermore, the f_Q evolution in low density environment suggest the existence of internal environment-independent quenching mechanisms.

5. By fitting our f_Qs, we illustrate that f_Q in high density environments is greater than f_Q in low density environments regardless of mass and redshift.

This result reflects the well known trend that galaxies in high density environment are statistically redder, have lower SFRs, and more massive.

6. Comparison of the $f_Q(\mathcal{M}_{fid})$ evolution for a range of environment classifications reveal that the since $z = 0.8$, f_Q has evolved by a greater amount in higher density environments. For our purest high environment sample ($n_{env} > 9$), the total f_Q evolution is ~ 0.1 greater than the total f_Q evolution in low density environment, revealing a moderate dependence in environment.

Many physical mechanisms have been proposed to explain the quenching of star-formation observed in our universe. Recently star-formation quenching has often been classified into internal or external mechanisms, and sometimes more specifically into mass-dependent and environment-dependent mechanisms (Baldry et al. 2006; Peng et al. 2010). The significant redshift evolution of the f_Q in low density environment confirms the existence of internal mechanisms that quench star-forming in galaxies.

Furthermore, the greater f_Q evolution in high density environment over low density environment demonstrates that in addition to the internal quenching mechanisms, in high density environments such as groups and clusters, environment-quenching also contributes to star-formation quenching. Although our results do not specifically shed light on which quenching mechanism (e.g. strangulation, ram-pressure stripping, etc.) occur in high density environments, they impose strict constraints on the total contribution of environment quenching that any environment quenching model must satisfy. More importantly, our results provide limit on the role of environment quenching in galaxy evolution.

REFERENCES

Abazajian, K. N., Adelman-McCarthy, J. K., Agüeros, M. A., et al. 2009, ApJS, 182, 543

Baldry, I. K., Balogh, M. L., Bower, R. G., et al. 2006, MNRAS, 373, 469

Behroozi, P. S., Marchesini, D., Wechsler, R. H., et al. 2013, ApJ, 777, L10

Bell, E. F., Papovich, C., Wolf, C., et al. 2005, ApJ, 625, 23

Bernardi, M., Meert, A., Sheth, R. K., et al. 2013, MNRAS, 436, 697

Blanton, M. R., Eisenstein, D., Hogg, D. W., & Zehavi, I. 2006, ApJ, 645, 977

Blanton, M. R., Kazin, E., Muna, D., Weaver, B. A., & Price-Whelan, A. 2011, AJ, 142, 31

Blanton, M. R., & Moustakas, J. 2009, ARA&A, 47, 159

Blanton, M. R., Schlegel, D. J., Strauss, M. A., et al. 2005, AJ, 129, 2562

Bolzonella, M., Kovač, K., Pozzetti, L., et al. 2010, A&A, 524, A76

Borch, A., Meisenheimer, K., Bell, E. F., et al. 2006, A&A, 453, 869

Bundy, K., Ellis, R. S., Conselice, C. J., et al. 2006, ApJ, 651, 120

Butcher, H., & Oemler, Jr., A. 1984, ApJ, 285, 426

Chabrier, G. 2003, PASP, 115, 763

Coil, A. L., Blanton, M. R., Burles, S. M., et al. 2011, ApJ, 741, 8

Conroy, C., & Gunn, J. E. 2010, FSPS: Flexible Stellar Population Synthesis, astrophysics Source Code Library, ascl:1010.043

Cool, R. J., Moustakas, J., Blanton, M. R., et al. 2013, ApJ, 767, 118

Cooper, M. C., Newman, J. A., Madgwick, D. S., et al. 2005, ApJ, 634, 833

Cooper, M. C., Newman, J. A., Weiner, B. J., et al. 2008, MNRAS, 383, 1058

Cooper, M. C., Coil, A. L., Gerke, B. F., et al. 2010, MNRAS, 409, 337

Croton, D. J., Farrar, G. R., Norberg, P., et al. 2005, MNRAS, 356, 1155

Cucciati, O., Iovino, A., Kovač, K., et al. 2010, A&A, 524, A2

Desai, V., Dalcanton, J. J., Aragón-Salamanca, A., et al. 2007, ApJ, 660, 1151

Dressler, A. 1980, ApJ, 236, 351

Dressler, A. 1984, ARA&A, 22, 185

Geha, M., Blanton, M. R., Yan, R., & Tinker, J. L. 2012, ApJ, 757, 85

Guzzo, L., Strauss, M. A., Fisher, K. B., Giovanelli, R., & Haynes, M. P. 1997, ApJ, 489, 37

Hermit, S., Santiago, B. X., Lahav, O., et al. 1996, MNRAS, 283, 709

Hopkins, A. M., & Beacom, J. F. 2006, ApJ, 651, 142

Hubble, E. P. 1936, The Realm of the Nebulae (New Haven: Yale University Press)

Iovino, A., Cucciati, O., Scodeggio, M., et al. 2010, A&A, 509, A40

Jarrett, T. H., Chester, T., Cutri, R., et al. 2000, AJ, 119, 2498

Johnston, R. 2011, A&A Rev., 19, 41

Kovač, K., Lilly, S. J., Knobel, C., et al. 2010, ApJ, 718, 86

—. 2014, MNRAS, 438, 717

Leja, J., van Dokkum, P., & Franx, M. 2013, ApJ, 766, 33

Magnelli, B., Elbaz, D., Chary, R. R., et al. 2009, A&A, 496, 57

Markwardt, C. B. 2009, in Astronomical Society of the Pacific Conference Series, Vol. 411, Astronomical Data Analysis Software and Systems XVIII, ed. D. A. Bohlender, D. Durand, & P. Dowler, 251

Martin, D. C., Fanson, J., Schiminovich, D., et al. 2005, ApJ, 619, L1

McCarthy, I. G., Frenk, C. S., Font, A. S., et al. 2008, MNRAS, 383, 593

Morrissey, P., Schiminovich, D., Barlow, T. A., et al. 2005, ApJ, 619, L7

Moustakas, J., Coil, A. L., Aird, J., et al. 2013, ApJ, 767, 50

Muldrew, S. I., Croton, D. J., Skibba, R. A., et al. 2012, MNRAS, 419, 2670

Noeske, K. G., Weiner, B. J., Faber, S. M., et al. 2007, ApJ, 660, L43

Oemler, A. 1974, ApJ, 194, 1

Patel, S. G., Holden, B. P., Kelson, D. D., Illingworth, G. D., & Franx, M. 2009, ApJ, 705, L67

Peng, Y.-j., Lilly, S. J., Kovač, K., et al. 2010, ApJ, 721, 193

Pozzetti, L., Bolzonella, M., Zucca, E., et al. 2010, A&A, 523, A13

Salim, S., Rich, R. M., Charlot, S., et al. 2007, ApJS, 173, 267

Scodeggio, M., Vergani, D., Cucciati, O., et al. 2009, A&A, 501, 21

Swanson, M. E. C., Tegmark, M., Hamilton, A. J. S., & Hill, J. C. 2008, MNRAS, 387, 1391

Tasca, L. A. M., Kneib, J.-P., Iovino, A., et al. 2009, A&A, 503, 379

Taylor, E. N., Franx, M., van Dokkum, P. G., et al. 2009, ApJ, 694, 1171

Tinker, J., Wetzel, A., & Conroy, C. 2011, ArXiv e-prints, arXiv:1107.5046

Wilman, D. J., Zibetti, S., & Budavári, T. 2010, MNRAS, 406, 1701

York, D. G., Adelman, J., Anderson, Jr., J. E., et al. 2000, AJ, 120, 1579